JOURNAL OF THERMOPHYSICS AND HEAT TRANSFER
Vol. 9, No. 2, April–June 1995

Dynamic Behavior of an Unheated Meniscus Subjected to Transient Acceleration Field

Kirk L. Yerkes*
U.S. Air Force Wright Laboratory, Wright–Patterson Air Force Base, Ohio 45433-7251
and
Kevin P. Hallinan†
University of Dayton, Dayton, Ohio 45469-0210

This study experimentally and analytically investigates the effects of acceleration transients on the dynamic response of an unheated meniscus in a capillary tube. A capillary tube partially filled with either water or ethyl alcohol was mounted on a centrifuge to observe the dynamic response of the meniscus subject to an acceleration transient. It was found that for a transverse acceleration component of less than 2 *g*, experimental data of the meniscus advance or recession agreed well with a one-dimensional formulation of the equation of motion that assumed a spherical-shaped meniscus. However, for a transverse acceleration greater than 2 *g*, there was an increase in the observed meniscus velocity, both upon recession and advancement, resulting in a lower meniscus position when compared to the analytically predicted position. Water exhibited a significant amount of "sticking" and hysteresis that appeared to intensify with increasing transverse acceleration.

Nomenclature

a = capillary tube radius
B = coefficient defined by Eqs. (11) and (12)
Bo = Bond number, $(2a)^2 g_{pk}\rho/\sigma$
$\bar{b}$ = acceleration vector
Ca = capillary number, $\mu V_c/\sigma$
$\hat{e}$ = unit vector
$\bar{F}$ = force vector
g = gravitational acceleration
g_{pk} = peak radial acceleration component
h_0 = static wicking height, $2\sigma \cos\theta/\rho a g \sin\phi$
m = mass of liquid column in inclined capillary tube
Re = Reynolds number, $(2a)\rho V_c/\mu$
r = radial coordinate
r_0' = radial location of capillary tube pivot point
t = time
tf = angular velocity cycle period
$\bar{t}^{(n)}$ = surface traction vector
$\bar{V}$ = velocity vector
V_c = characteristic velocity, $2h_0/tf$
v = velocity component
z = capillary tube axial directional coordinate
z_1 = capillary tube axial pivot location
ζ = dimensionless meniscus position, η/h_0
η = meniscus position
Θ = dimensionless time, t/tf
θ = equivalent contact angle
μ = dynamic viscosity
ρ = density
σ = surface tension
$\bar{\sigma}$ = stress tensor
τ_w = wall shear stress
ϕ = inclination angle
Ω = angular velocity as a function of Θ
ω = angular velocity

Subscripts
ave = average
b = body
R = capillary tube transverse direction
r_T = centrifuge radial direction
s = surface
T = centrifuge tangential direction
y = vertical direction
z = capillary tube axial direction

Introduction

THE static and dynamic behavior of two- and three-phase interfaces constitute a range of problems that have been frequently addressed by investigators over the last several years.[1–3] These interfaces, which may be referred to as contact lines, often involve the displacement of one immiscible fluid in another along a solid surface, the spreading of a liquid drop on a solid, the displacement of gas or vapor by a liquid in a capillary tube, etc.

There are many processes that require information with regard to the static and dynamic behavior of contact lines, such as the spreading of viscous liquids like paint, adhesive technologies, lubrication technologies, oil recovery, and processes utilizing contact lines and capillarity to enhance heat and mass transfer. The latter relates to condensation and evaporation processes associated with a wetting liquid on planar surfaces and within wicking structures consisting of porous media, grooved structures, and screens. In these cases, it is typical to have length-scales associated with the size of droplets, grooves, or pores on the order of several millimeters or less, resulting in a dominant surface tension force that controls the shape of the fluid-fluid interface close to the contact line.

Additional difficulties arise when devices incorporating these processes are subjected to elevated steady-state and transient acceleration fields. Elevated steady-state acceleration fields resulting in forces on the same order of magnitude or greater than surface tension forces may affect the shape of the fluid interface. Transient acceleration-induced forces (both transverse and axial), in addition to altering the fluid interface shape, will cause motion of the contact line as the acceleration potential associated with the liquid filled pore or groove changes. In such instances, the contact line velocity is functionally dependent on these transient acceleration-induced forces as well

Received June 28, 1994; revision received Oct. 19, 1994; accepted for publication Oct. 20, 1994. This paper is declared a work of the U.S. Government and is not subject to copyright protection in the United States.

*Research Engineer, WL/POOS-3, Aero Propulsion and Power Directorate. Student Member AIAA.
†Associate Professor, Department of Mechanical Engineering.

as surface tension. The inclusion of these elevated steady-state and transient acceleration fields defines a class of problems that are unique in the study of the static and dynamic behavior of contact lines.

If the problem of a static meniscus in a capillary tube is considered (discounting the near contact line region where the solid-liquid intermolecular forces may dominate the force field at the fluid interface), the equilibrium equation

$$\nabla \cdot \bar{\sigma} + \rho \bar{b} = 0 \tag{1}$$

must be satisfied. A traction stress vector boundary condition in terms of surface tension is imposed on the free-surface interface. If this interface is assumed to have a spherical shape

$$\bar{t}^{(\hat{n})} \cdot \hat{n} = \sigma / R_m \tag{2}$$

is also satisfied. With this assumption, the "apparent" contact angle at the contact line is also required as a boundary condition to determine the radius of curvature, and therefore, the interface shape. The specification of an apparent contact angle is intended to macroscopically describe the contribution of the physics of the extended meniscus region.

Concus[4] investigated the effect of Bond number on the shape of this interface in a right circular cylinder. Several contact angles were specified and the equilibrium equation was solved for the interface shape as a function of contact angle. His results showed that the interface shape was not necessarily spherical in nature, but was strongly dependent on the specified contact angle and corresponding Bond number.

Several different approaches, either macroscopic or microscopic, have been used to describe the dynamics associated with an advancing or receding meniscus. In the macroscopic approach, the details of the near contact line region are ignored. For example, Calvo et al.[5] examined the advancing meniscus in a horizontal capillary tube attached to a liquid reservoir. It was found that the advance of the meniscus was controlled by 1) the gravity head of the liquid above the capillary tube and 2) the line force associated with the apparent contact line equal to $2\sigma/r \cos \theta_d$, where θ_d is the apparent contact line angle for dynamic conditions. Their results indicated that for capillary numbers less than 10^{-5}, $\theta_d \approx \theta_s$, the static contact angle. With increasing capillary numbers the dynamic contact angle increases for advancing menisci and decreases for receding menisci. The macroscopic predictions of the advancing rate of the meniscus showed good agreement with experimental data.

The microscopic approach has focused on the details of the thin film region near the contact line. Instead of prescribing a line force, this approach has sought to determine the total dissipation in the thin film where the velocity gradients will be maximum. Thus, the viscous losses in the thin film will control the motion of the meniscus. In particular, de Gennes et al.[6] considered the dynamic behavior of the contact line associated with the spreading of a partially wetting fluid on an inclined moving plate. They differentiated the physics of the thin film region from that associated with the intrinsic meniscus region by accounting for the cumulative effect of solid–liquid internal forces in the thin film through the disjoining pressure concept. Gradients in the disjoining pressure were observed to be the "driver" for the near contact line flow.

Ngan and Dussan[7] and Dussan et al.[8] ignored the details of the thin film region (called the inner region in their terminology), recognizing that this inner region while unaffected by the outer region (the intrinsic meniscus region) did, in fact, influence the outer region through its role in determining the apparent contact angle. They used a matched asymptotic analysis, that in an intermediate region there was a "material" actual contact angle from which an asymptotic solution could be derived to determine the macroscopic apparent contact angle. Experimental verification of this material actual contact angle agreed well with the theoretical predictions.

To date, both the microscopic and macroscopic formulations have been limited to situations where the Bond number is small (e.g., inside of capillary tubes) or where it is infinite (such as exists for draining films[9]). While acceleration-induced forces are considered conservative and long-range in nature, they affect the free-surface shape and the slope for which solutions to the subregions as described by de Gennes et al.[6] must be asymptotically matched. Furthermore, it is not known what potential effects these forces may have on the precursor film thickness and stability in both static and dynamic conditions.

In general, prior investigations with regard to the dynamic behavior of the contact line have specified a contact line velocity consistent with a moving solid boundary. Transient acceleration-induced forces will induce a contact line velocity posing a problem such that the contact line dynamics are dependent only on the temporal acceleration fields and not on a moving solid boundary. There has been limited research with regard to the effects of acceleration-induced forces. Most of these have addressed the equilibrium free-surface shape.[4] This article discusses the dynamic behavior of the meniscus and contact line region in a capillary tube subjected to a transient acceleration field.

Experimental

Acceleration Field

Transient acceleration fields were generated using a 2.4-m-diam centrifuge table (Fig. 1) rotating with a time variant angular velocity. Angular velocity transients were generated at a specified cyclic frequency of 0.0015 Hz (tf = 1/0.0015 s) using a signal or waveform generator as a control input to the centrifuge. The angular velocity was increased linearly to a peak value at the midpoint of the cycle and subsequently decreased. A tri-axis accelerometer (Columbia Research Laboratories, Inc.) was used to monitor the time variant acceleration components in a Cartesian reference frame affixed to the centrifuge table. For this investigation, the peak angular velocity was specified such that a 4.2-g ± 0.1-g peak radial acceleration was generated (g_{pk} = 41.20 m/s^2).

Capillary Test Cell

A sealed test cell containing a glass capillary tube and reservoir was positioned on the centrifuge as shown in Fig. 2. The test cell was mounted to a motorized optics rotation stage (Newport) such that the capillary tube was allowed to pivot about its c.m. This pivot point was displaced vertically from

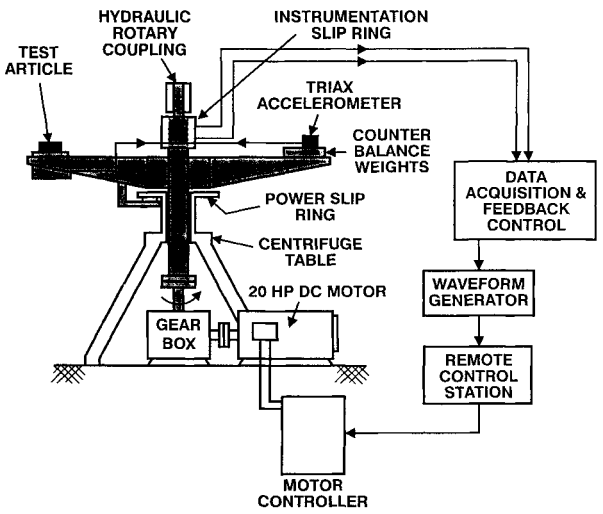

Fig. 1 Schematic of centrifuge.

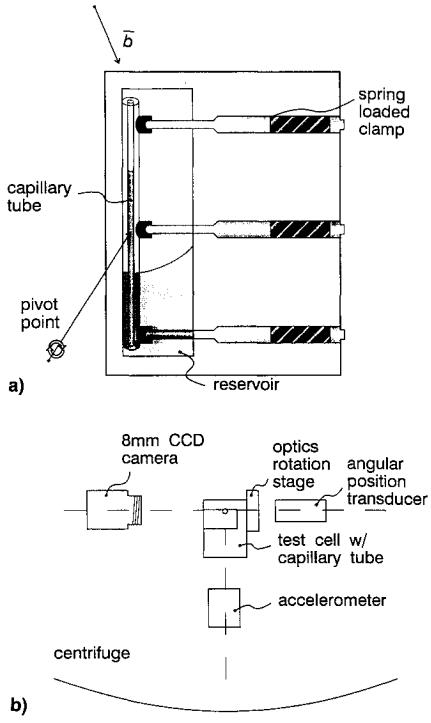

Fig. 2 Experimental apparatus: a) sealed test cell and b) schematic of experimental apparatus as mounted on the centrifuge.

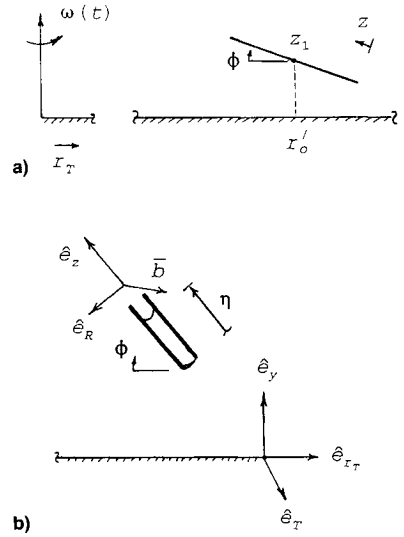

Fig. 3 Capillary tube orientation: a) pivot point location, directional coordinates and b) coordinate systems as referenced to the centrifuge accelerometer and capillary tube.

the centrifuge surface at a fixed radial location r_0' as shown in Fig. 3a. Angles of inclination of the capillary tube were determined from the output of a calibrated angular position transducer (Trans-Tek, Inc.) accurate to within ± 0.2 deg.

Experiments were conducted by fixing the capillary tube at a specified inclination angle while subjecting it to the transient acceleration field. Increasing the inclination angle elevates the transverse acceleration component referenced to the capillary tube. This allowed the dynamic response of the meniscus subjected to an increasing transverse acceleration component to be observed experimentally. The dynamic response of the meniscus to the transient acceleration field was observed using an 8-mm CCD camera (Sony) mounted adjacent to the test cell as shown in Fig. 2b. The meniscus height relative to the reservoir meniscus η was measured as a function of time to within ± 1.0 mm. An equivalent contact angle θ was calculated from the experimentally determined static wicking height h_0 for conditions when the transverse acceleration component was zero

$$h_0 \rho g \approx (2\sigma/a)\cos\,\theta$$

Water (reverse osmosis) and ethyl alcohol were used as the test fluids to demonstrate the importance of the equilibrium contact angle on the advance and recession of the meniscus due to a transient acceleration field. Properties of these fluids were assumed to be that of the bulk fluid corresponding to a experimental temperature of 30°C.

The test cell and capillary tube were cleaned using potassium hydroxide and rinsed with distilled water. The test cell was filled and subsequently sealed resulting in a fill that had a combination of air, fluid vapor, and fluid.

Analytical Formulation

The goals of the analytical formulation were as follows:

1) Mathematically describe the transient nature of the acceleration field referenced to the capillary tube in the meniscus region.

2) Mathematically describe the dynamic behavior of the meniscus as a result of the temporal acceleration-induced forces using a simplified one-dimensional model with a constant line force.

3) Infer the relative importance of the transverse acceleration component, Bond number, and capillary number on the meniscus motion by comparing experimental results and analytical calculations.

Acceleration Vector

Acceleration measurements were obtained with regard to a three-dimensional Cartesian noninertial reference frame affixed to the centrifuge. The acceleration field was then referenced to fixed locations on the capillary tube and subsequently decomposed into transverse and axial acceleration components relative to the capillary tube as shown in Fig. 3b.

The transient acceleration vector in a Cartesian coordinate reference frame from the viewpoint of an observer on the centrifuge is of the form

$$\tilde{\boldsymbol{b}} = b_{r_T}\hat{\boldsymbol{e}}_{r_T} + b_y\hat{\boldsymbol{e}}_y + b_T\hat{\boldsymbol{e}}_T = b_z\hat{\boldsymbol{e}}_z + b_R\hat{\boldsymbol{e}}_R \qquad (3)$$

where for a fixed radial location r_T the following radial, tangential, and vertical acceleration components are realized:

$$b_{r_T}(t) = \omega^2(t) r_T, \qquad b_T(t) = \frac{d\omega(t)}{dt} r_T, \qquad b_y(t) = -g$$

After an appropriate transformation to the capillary tube reference frame, the acceleration vector can be decomposed into an axial component b_z and a transverse component b_R, which results in

$$\tilde{\boldsymbol{b}} = \{-\omega^2[r_0' + (z_1 - z)\cos\,\phi]\cos\,\phi + (-g)\sin\,\phi\}\hat{\boldsymbol{e}}_z + \left(\{-\omega^2[r_0' + (z_1 - z)\cos\,\phi]\sin\,\phi - (-g)\cos\,\phi\}^2 + \left\{[r_0' + (z_1 - z)\cos\,\phi]\frac{d\omega}{dt}\right\}^2\right)^{1/2}\hat{\boldsymbol{e}}_R \qquad (4)$$

Here, the transverse component b_R is a magnitude with no reference to direction due to the axisymmetric nature of the capillary tube.

Equation of Motion

A simple analytical model is described that predicts the motion of the meniscus subjected to transient accelerations. The analytical formulation of the equation of motion was simplified assuming bulk flow only in the axial direction of

the capillary tube. Effectively, the liquid column in the capillary tube is assumed to undergo a slug flow. From the conservation of momentum

$$\sum \bar{F} = \bar{F}_s + \bar{F}_b = \frac{d(m\bar{V})}{dt} \tag{5}$$

the surface and body forces in the axial direction combine, resulting in the axial force

$$F_z = F_{s_z} + F_{b_z} \tag{6}$$

The surface force F_{s_z} is formulated by accounting for the cumulative effect of solid–liquid intermolecular forces in the near contact line region and the wall shear stress associated with Poiseuille flow in the liquid column. The contact line force is defined assuming a spherical meniscus and a constant equivalent or apparent contact angle such that

$$F_{s_z} = \sigma(2\pi a)\cos\theta + \tau_w(2\pi a)\eta \tag{7}$$

Note that such an assumption implies a nonchanging apparent contact angle under dynamic conditions. A great deal of work has established a relationship between the dynamic contact angle θ_d and the capillary number (for low Bond numbers) as summarized by Hoffman.[10] These results have shown little change in the contact angle for capillary numbers less than 10^{-5}.

The shear stress at the wall outside the contact line region is defined using the Darcy friction factor assuming laminar tube flow where

$$\tau_w = 64/Re(\rho V_{ave}^2/8) \tag{8}$$

Using a slug flow approximation to describe the flow of liquid in the column, i.e., $V_{ave} = d\eta/dt$, the surface force formulation becomes

$$F_{s_z} = \sigma(2\pi a)\cos\theta - 8\pi\mu\eta\frac{d\eta}{dt} \tag{9}$$

The total body force

$$F_{b_z} = \int_0^\eta \int_0^a b_z\rho(2\pi)r\,dr\,dz \tag{10}$$

is formulated by integrating over the volume of the liquid column the axial acceleration component b_z [defined in Eq. (4)]. In the expression for b_z, the transient angular velocity is of the form

$$\begin{aligned}\omega(t) &= Bt, \qquad 0 \le t \le (tf/2)\\ &= B(tf - t), \qquad (tf/2) \le t \le tf\end{aligned} \tag{11}$$

where

$$B = [4g_{pk}/(tf)^2 r_0']^{1/2} \tag{12}$$

Assuming that the axial fluid velocity is also defined by $v_z = d\eta/dt$ (due to the slug flow assumption), and the mass in the capillary tube as $m = \rho(\pi a^2)\eta$, the relation for the time rate of change in momentum is defined as

$$\frac{d(mv_z)}{dt} = \rho(\pi a^2)\left[\eta\frac{d^2\eta}{dt^2} + \left(\frac{d\eta}{dt}\right)^2\right] \tag{13}$$

Combining Eqs. (9), (10), and (13), the momentum equation becomes

$$\left(\frac{2\sigma\cos\theta}{\rho a}\right) - \left(\frac{8\mu}{\rho a^2}\eta\frac{d\eta}{dt}\right) + \left(\int_0^\eta b_z\,dz\right) = \left[\eta\frac{d^2\eta}{dt^2} + \left(\frac{d\eta}{dt}\right)^2\right] \tag{14}$$

Integrating the axial acceleration term b_z, and rearranging, the momentum equation becomes

$$\frac{2\sigma\cos\theta}{\rho a} = \left[\eta\frac{d^2\eta}{dt^2} + \left(\frac{d\eta}{dt}\right)^2\right] + \left[\frac{8\mu}{\rho a^2}\eta\frac{d\eta}{dt}\right] + \eta\left\{\omega(t)^2\cos\phi\left[\left(z_1 - \frac{\eta}{2}\right)\cos\phi + r_0'\right] + g\sin\phi\right\} \tag{15}$$

A nondimensional form of the momentum equation can now be derived using the following dimensionless parameters:

$$\begin{aligned}\zeta &= \eta/h_0, \qquad 0 \le \zeta \le 1\\ \Theta &= t/tf, \qquad 0 \le \Theta \le 1\end{aligned} \tag{16}$$

with the following initial conditions:

$$\zeta = 1, \qquad \frac{d\zeta}{d\Theta} = 0, \qquad \Theta = 0$$

A new angular velocity Ω is formed by factoring g_{pk} out of the coefficient B [defined by Eq. (12)] in Eq. (11) and casting it in terms of the nondimensional time Θ, where

$$\begin{aligned}\Omega(\Theta) &= (4/r_0')^{1/2}\Theta, \qquad 0 \le \Theta \le \tfrac{1}{2}\\ &= (4/r_0')^{1/2}(1 - \Theta), \qquad \tfrac{1}{2} \le \Theta \le 1\end{aligned} \tag{17}$$

The nondimensional form of the momentum equation becomes

$$\frac{g}{g_{pk}}\sin\phi = \left(\frac{a}{h_0}\right)\left(\frac{ReCa}{2Bo}\right)\left[\zeta\frac{d^2\zeta}{d\Theta^2} + \left(\frac{d\zeta}{d\Theta}\right)^2\right] + \left(\frac{16Ca}{Bo}\right)\left(\zeta\frac{d\zeta}{d\Theta}\right) + \zeta\left\{\Omega(\Theta)^2\cos\phi \times \left[\left(z_1 - \frac{h_0\zeta}{2}\right)\cos\phi + r_0'\right] + \frac{g}{g_{pk}}\sin\phi\right\} \tag{18}$$

The first and second terms of Eq. (18) represent the inertial and viscous effects, respectively, with the coefficients formed as the products of the dimensionless parameters of Reynolds, capillary, and Bond numbers. The Reynolds and capillary numbers are referenced to a characteristic velocity V_c, which is the maximum attainable velocity over one-half of the acceleration cycle period, assuming $\eta = 0$ at g_{pk}. The Bond number is referenced to the peak radial acceleration component g_{pk}.

For small inertial and viscous effects, the momentum equation can be reduced to the following quadratic form for the transient dimensionless meniscus position:

$$\zeta^2 - \left[\frac{\Omega(\Theta)^2\cos\phi(z_1\cos\phi + r_0') + (g/g_{pk})\sin\phi}{\Omega(\Theta)^2(h_0/2)\cos^2\phi}\right]\zeta + \left[\frac{(g/g_{pk})\sin\phi}{\Omega(\Theta)^2(h_0/2)\cos^2\phi}\right] = 0 \tag{19}$$

Results

Equations (18) and (19) were solved for the dimensionless meniscus position using a central difference scheme and as a quadratic, respectively. These solutions were obtained as a result of specifying a static wicking height h_0 based on the experimentally determined equivalent contact angle θ. Solutions to Eqs. (18) and (19) were identical for the experimental parameter range specified in this investigation. This supports the use of the closed form solution of Eq. (19) in instances where inertial and viscous effects can be assumed to be negligible.

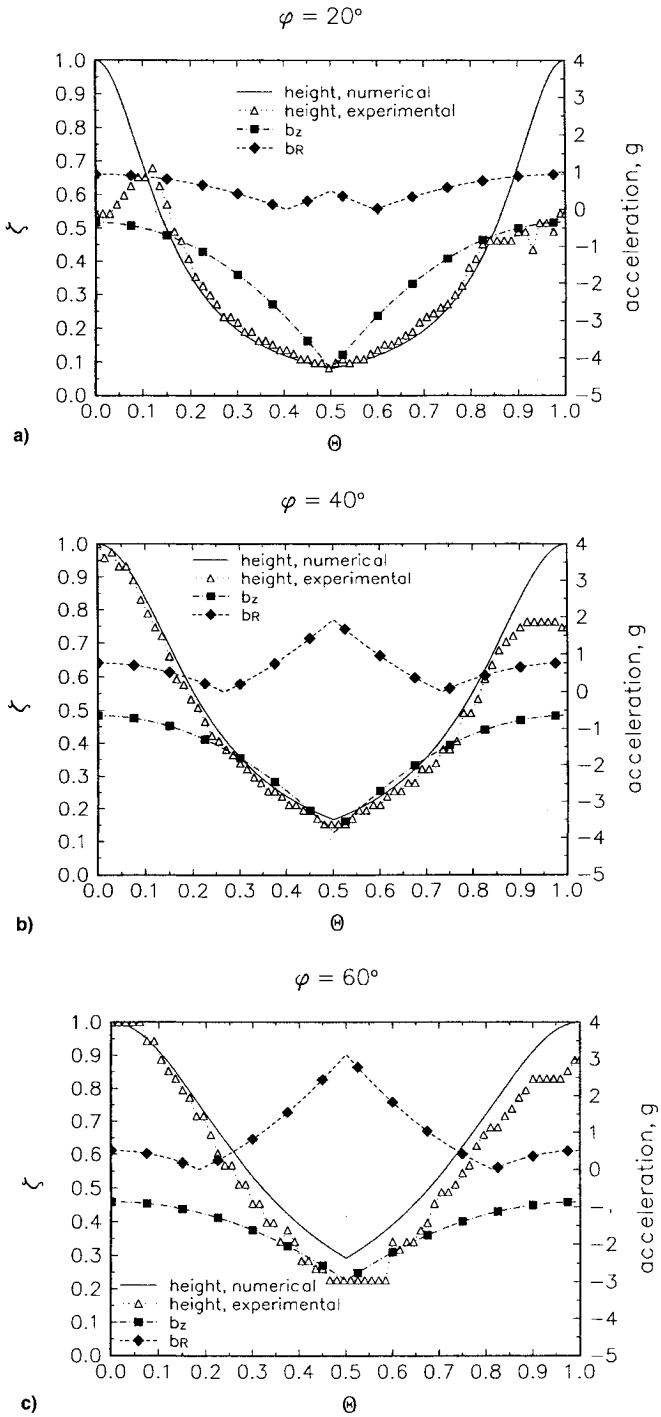

Fig. 4 Experimental data compared to analytical results for water at Bo = 2.05: a) ϕ = 20 deg, Ca = 1.50 × 10^{-6}, Re = 0.278, a/h_0 = 2.25 × 10^{-2}; b) ϕ = 40 deg, Ca = 7.99 × 10^{-7}, Re = 0.148, a/h_0 = 4.24 × 10^{-2}; and c) ϕ = 60 deg, Ca = 5.93 × 10^{-7}, Re = 0.110, a/h_0 = 5.71 × 10^{-2}.

Experiments were performed and the results compared with solutions to the analytical model. Uncertainty in experimentally obtained ζ and Θ was on the order of ζ, $\Theta \pm 0.02$ based on the accuracy and resolution of experimentally measured quantities. In general, the comparison between the model and the experiment is surprisingly good, given the simplicity of the model. However, a number of interesting deviations from the model help to provide insight into the physical phenomena associated with the advancing/receding meniscus.

Figure 4 compares the experimentally obtained dimensionless meniscus position to the analytical results for water at varying angles of inclination. Also shown are the axial and transverse acceleration components. The equivalent contact angle was 22.2 deg with an experimental Bond number of 2.05. Experimental parameters ranged from $5.9 \times 10^{-7} \leq Ca \leq 1.5 \times 10^{-6}$, $0.11 \leq Re \leq 0.28$, and $2.3 \times 10^{-2} \leq a/h_0 \leq 5.7 \times 10^{-2}$ as the inclination angle varied from 20 to 60 deg.

There was a significant amount of "sticking" of the advancing meniscus for water as evidenced by the discontinuous nature of the meniscus position curves, Fig. 4. There also was a permanent hysteresis in the meniscus position at the completion of the test cycle resulting in a lower wicking height. This sticking of the meniscus appeared to become more significant with an increased transverse acceleration component, as demonstrated in Fig. 4c. For a peak transverse acceleration component greater than 2.5 g, the experimental results showed an increase in the meniscus velocity for both the receding and advancing meniscus from that predicted by the analytical results, Fig. 4c. At the midpoint of the acceleration cycle the meniscus position was also lower in Figs. 4d and 4c than that predicted analytically.

Also, for all cases using water as the test fluid, the initial meniscus recession speed tended to be underpredicted. Since the contact line force in the predictions is controlling the receding and advancing velocities it is apparent that it is slightly overpredicting the actual contact line dissipation. Using an equivalent contact angle to describe the line force at the contact line neglects the fact that, as the meniscus recedes, some fluid is left behind rather than being dragged over the tube wall.[9] Thus, the line force is physically less than predicted by the model. Conversely, for the advancing contact line, since it is presumed that a film of liquid is already present on the i.d. of the tube, it is easier for the meniscus to advance relative to that predicted for an advancing meniscus over a dry surface (such as is associated with using the equivalent contact angle).

Figure 5 compares the experimentally obtained dimensionless meniscus position to the analytical results for ethyl alcohol at varying angles of inclination. As with Fig. 4, also shown are the axial and transverse acceleration components. The equivalent contact angle was 16.7 deg with an experimental Bond number of 1.47. Experimental parameters ranged from $1.7 \times 10^{-6} \leq Ca \leq 3.6 \times 10^{-6}$, $3.0 \times 10^{-2} \leq Re \leq 6.1 \times 10^{-2}$, and $1.9 \times 10^{-2} \leq a/h_0 \leq 4.0 \times 10^{-2}$.

The experimentally obtained dimensionless meniscus position for ethyl alcohol agrees well with the analytical results to within experimental error for a peak transverse acceleration component less than 2 g. No sticking of the meniscus was observed and there was no observable hysteresis. As shown in Figs. 5b and 5c, there was an observable increase in the meniscus velocity relative to the model for both the receding and advancing meniscus for a peak transverse acceleration component greater than 2 g. This increase in meniscus velocity resulted in a meniscus position lower than that predicted analytically.

The effects of capillary number for a fixed Bond number and inclination angle on the dimensionless meniscus position are shown in Fig. 6. A comparison of the analytical results, using Eq. (18), for a Bond number of 0.42 and capillary numbers of 10^{-6}, 10^{-5}, and 10^{-4} at a 20-deg inclination angle demonstrates that, for capillary numbers less than 10^{-5}, vis-

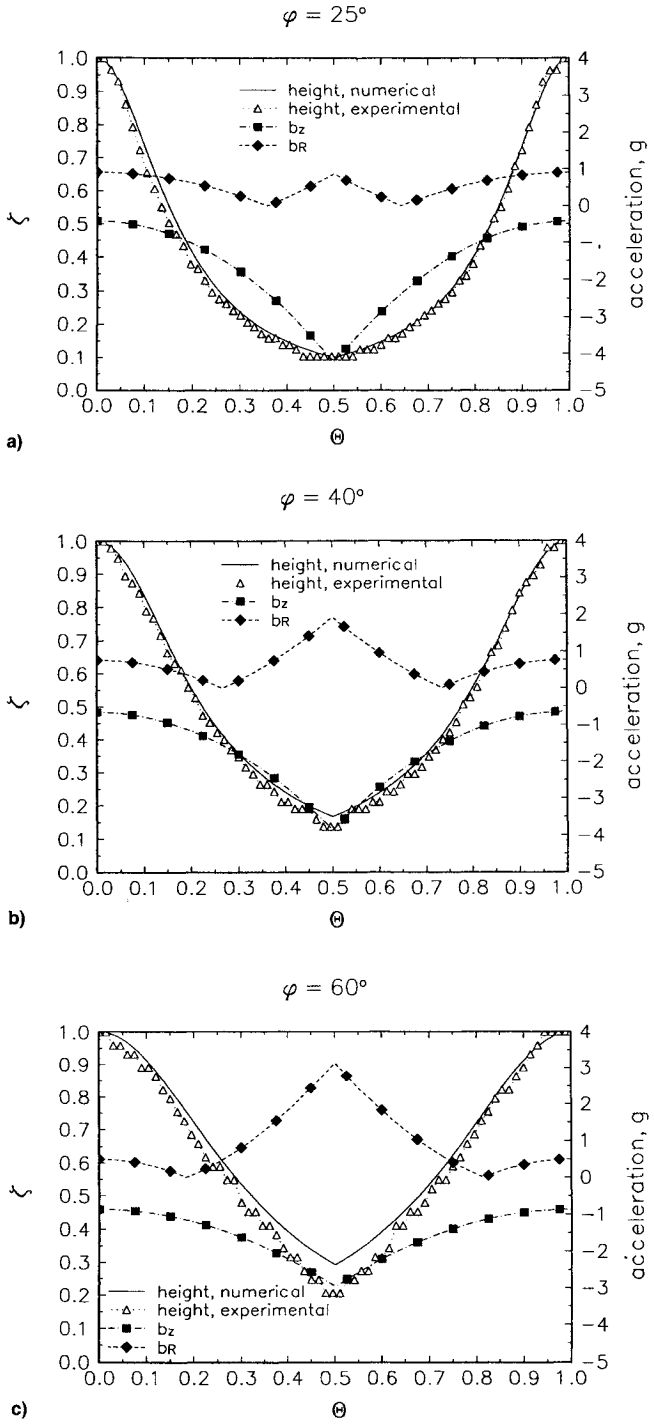

Fig. 5 Experimental data compared to analytical results for ethyl alcohol at Bo = 1.47: a) ϕ = 25 deg, Ca = 3.55 × 10^{-6}, Re = 6.07 × 10^{-2}, a/h_0 = 1.93 × 10^{-2}; b) ϕ = 40 deg, Ca = 2.33 × 10^{-6}, Re = 3.98 × 10^{-2}, a/h_0 = 2.94 × 10^{-2}; and c) ϕ = 60 deg, Ca = 1.73 × 10^{-6}, Re = 2.96 × 10^{-2}, a/h_0 = 3.96 × 10^{-2}.

cous losses outside of the contact line had only a small effect on the meniscus position. However, for capillary numbers on the order of 10^{-4} and greater, there is a significant lag in the meniscus position due to viscous effects. Capillary numbers less than 10^{-5} and Bond numbers ranging from 0.42 to 2.1 were predicted to have no effect on the dynamic response of the meniscus.

Analytical results, using Eq. (18), for a capillary number of 10^{-4} and Bond numbers of 0.42, 0.84, and 1.26 at angles of inclination ranging from 20 to 60 deg, are compared in Fig. 7. Figure 7a shows the dimensionless meniscus position at varying angles of inclination for a fixed Bond number of 0.42

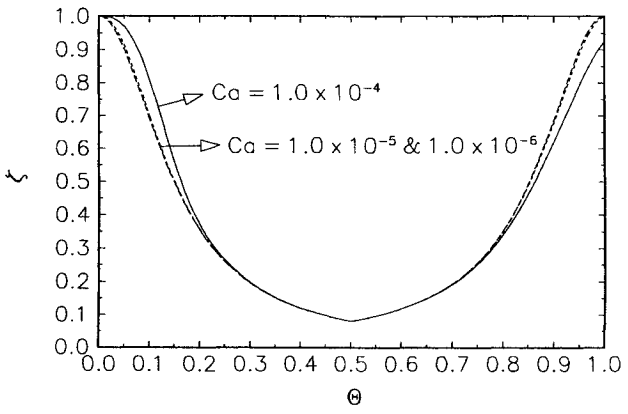

Fig. 6 Analytical results for ϕ = 20 deg, Bo = 0.42, and varying capillary number.

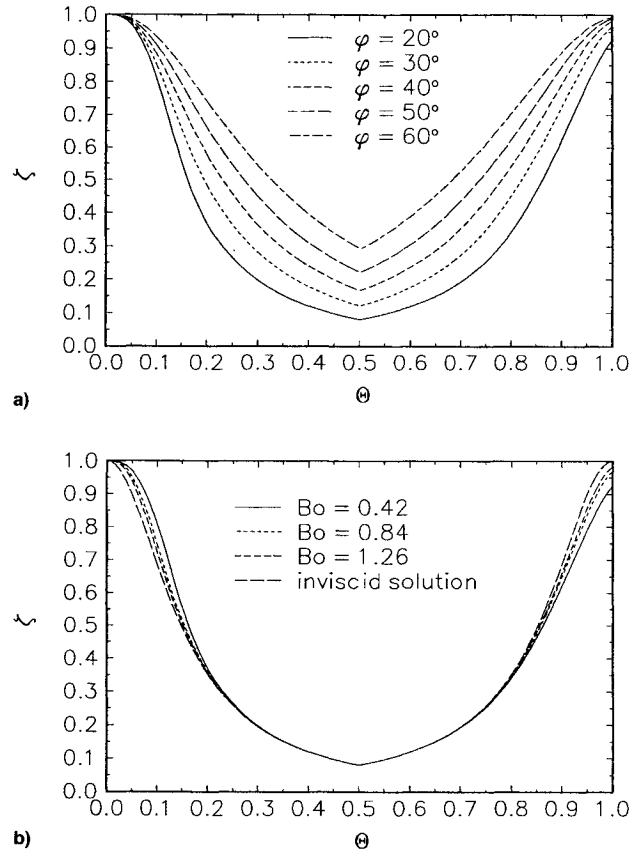

Fig. 7 Analytical results: a) varying angle of inclination (Bo = 0.42, Ca = 1.0 × 10^{-4}) and b) varying Bond number (ϕ = 20 deg, Ca = 1.0 × 10^{-4}).

(recall that the Bond number is based on g_{pk}) and a capillary number of 10^{-4}. For decreasing angles of inclination, viscous effects outside the contact line region become significant resulting in the characteristic lag in meniscus position. These analytical results do not take into account the significance of the transverse acceleration component at the higher angles of inclination and to the extent at which this transverse component affects the dynamic response of the meniscus. Figure 7b compares the dimensionless meniscus position for a varying Bond number with that of the inviscid solution, using Eq. (19), neglecting inertial effects at a 20-deg inclination angle. Here, a decrease in Bond number resulted in the increased importance of viscous effects yielding a lag in the meniscus position when compared to the low inertia inviscid solution. For Bond numbers less than 1.3 and capillary numbers greater than 10^{-4}, there were significant viscous effects resulting in a lag in the meniscus position. However, these results assume

a constant contact line force, as a result of specifying a constant equivalent contact angle, and do not account for the functional dependence of the contact angle on capillary number as discussed by Hoffman.[10] However, for experimental and analytical results with capillary numbers less than 10^{-5}, this dependence can be assumed to be negligible.

The magnitude of the transverse acceleration component had a significant effect on the dynamic response of the meniscus. This is in part attributed to the use of the constant equivalent contact angle to define a constant contact line force in the analytical formulation. While the meniscus shape may remain relatively spherical in nature, with an increased axial acceleration component for the relatively low Bond numbers considered, the transverse acceleration component will serve to reorient the meniscus in a transverse direction and distend it in the axial direction. This variation in the meniscus shape and position in the capillary tube will result in an increased contact line length that will tend to be elliptical rather than spherical. Therefore, one might expect an increase in the net contact line force due to the increased length of the contact line. Theoretically, the predicted recession and advancing rates would differ from those shown, actually moving in a direction opposite of that observed experimentally. Such observations point to the need for a closer examination of the near contact line region fluid physics with regard to the transverse acceleration component to completely describe the motion of the meniscus. Therefore, use of an equivalent contact angle to define the contact line force is an approximation at best. Instead, the contact angle, rather than being constant, is a function of the transverse acceleration component and angular position on the capillary tube wall.

Concluding Remarks

The dynamic response of an unheated meniscus within a capillary tube subjected to transient acceleration-induced forces was studied experimentally and analytically. Comparison of the experimental and analytical results showed that an elevated transverse acceleration greater than 2 g significantly altered the dynamic response of the meniscus and resulted in an increased meniscus velocity, and subsequently, lower meniscus position. It is speculated that this dynamic response in meniscus position is due to a reduced overall contact line force in the near contact line region resulting from the meniscus being moved in a transverse direction and distended in the axial direction.

The practical significance of these results, as related to heat transfer devices utilizing contact lines and capillarity to enhance heat and mass transfer, will be to provide information helpful in defining transient performance parameters and operational limits. It has long been assumed that the operating performance of such devices subjected to transverse acceleration components would not be altered significantly. However, as demonstrated in this study, the combined axial and transverse acceleration components may result in an increased depriming rate leading to a dryout condition sooner than typically predicted by conventional approaches. Also with the addition of heat, the deprime and reprime dynamics may be significantly altered and result in either a degraded or possibly improved performance such as with the arterial heat pipe discussed by Yerkes et al.[11]

References

[1]De Gennes, P. G., "Wetting: Statics and Dynamics," *Review of Modern Physics*, Vol. 57, 1985, pp. 827–863.

[2]Cazabat, A. M., "How Does a Droplet Spread?," *Contemporary Physics*, Vol. 28, 1987, pp. 347–364.

[3]Teletzke, G. F., Davis, H. T., and Scriven, L. E., "Wetting Hydrodynamics," *Revue De Physique Appliquee*, Vol. 23, 1988, pp. 989–1007.

[4]Concus, P., "Static Menisci in a Vertical Right Circular Cylinder," *Journal of Fluid Mechanics*, Vol. 34, No. 3, 1968, pp. 481–495.

[5]Calvo, A., Paterson, I., Chertcoff, R., Rosen, M., and Hulin, J. P., "Dynamic Capillary Pressure Variations in Diphasic Flows Through Glass Capillaries," *Journal of Colloid and Interface Science*, Vol. 141, No. 2, 1991, pp. 384–394.

[6]De Gennes, P. G., Hua, X., and Levinson, P., "Dynamics of Wetting: Local Contact Angles," *Journal of Fluid Mechanics*, Vol. 212, 1990, pp. 55–63.

[7]Ngan, C. G., and Dussan, V. E. B., "On the Dynamics of Liquid Spreading on Solid Surfaces," *Journal of Fluid Mechanics*, Vol. 209, 1989, pp. 191–226.

[8]Dussan, V. E. B., Ramé, E., and Garoff, S., "On Identifying the Appropriate Boundary Conditions at a Moving Contact Line: An Experimental Investigation," *Journal of Fluid Mechanics*, Vol. 230, 1991, pp. 97–116.

[9]Li, D., and Slattery, J. C., "Analysis of the Moving Apparent Common Line and Dynamic Contact Angle Formed by a Draining Film," *Journal of Colloid and Interface Science*, Vol. 143, No. 2, 1990, pp. 382–396.

[10]Hoffman, R. L., "A Study of the Advancing Interface I. Interface Shape in Liquid-Gas Systems," *Journal of Colloid and Interface Science*, Vol. 50, No. 2, 1975, pp. 228–240.

[11]Yerkes, K. L., Chang, W. S., and Beam, J. E., "Heat Pipe Performance with Transient Heat Flux and Body Force Effects," *Advances in Heat Pipe Science and Technology*, edited by M. Tongze, International Academic Publishers, Beijing, PRC, 1992, pp. 205–213.